PROCEEDINGS OF SCIENCE

Radar Echo Signals for RET-CR

Isha Loudon[a,*] **on behalf of the Radar Echo Telescope collaboration**
(a complete list of authors can be found at the end of the proceedings)

[a] *Université Libre de Bruxelles,*
1050 Brussels, Belgium
E-mail: isha.loudon@ulb.be

The goal of the Radar Echo Telescope (RET) collaboration is to detect ultra-high-energy (UHE) neutrinos via in-ice radar techniques. To this end, the RET collaboration aims to demonstrate the radar echo method in-situ with the Radar Echo Telescope for Cosmic Rays (RET-CR) experiment, located near Summit Station, Greenland. RET-CR utilised secondary in-ice particle cascades - generated by high-energy cosmic-ray air showers impacting the ice surface - as a test beam for the radar method. In this work, radar signals within a RET-CR detector configuration have been simulated using the semi-analytic simulation package MARES. The effects of different radar echo features on signal observables, including amplitude and frequency, have then been explored and linked to properties of the progenitor cosmic rays.

39th International Cosmic Ray Conference (ICRC2025)
15–24 July 2025
Geneva, Switzerland

*Speaker

PoS(ICRC2025)1104

1. Introduction

A high-energy particle interacting in ice produces a cascade of relativistic particles. As the cascade develops, it leaves behind a short-lived trail of ionisation. For sufficient densities, these trails allow for the particle cascade to be detected with radar: using in-ice radio frequency transmitters to illuminate the detection ice volume. Any particle cascade produced in the volume will then scatter a portion of the incident radio-frequency signal, producing a radar echo. The Radar Echo Telescope (RET) collaboration aims to utilise this radar method to detect UHE cosmic neutrinos with the future RET-N neutrino telescope. In this way, the radar echo signal can be used to establish properties of the neutrinos, providing insight into the particles themselves, as well as the energetic astrophysical processes that create them [1].

The radar detection method has been demonstrated in the T576 experiments undertaken at the Stanford Linear Accelerator (SLAC), resulting in the first observation of radar echoes from a particle cascade in dense media [2, 3]. The Radar Echo Telescope for Cosmic Rays (RET-CR) experiment represents the next step towards cosmic-neutrino detection with radar [4]. RET-CR aims to show the viability of the method in-situ through the detection of in-ice cascades generated by Cosmic-Ray (CR) air showers. A CR-EAS impacting a high-altitude ice surface produces a secondary in-ice particle cascade, similar to those produced by UHE neutrinos interacting in ice. The detection of these in-ice CR cascades will constitute strong evidence towards the use of the radar technique in neutrino detection with RET-N. RET-CR was deployed in the summer of 2023 and 2024, near Summit Station, Greenland [5], and analysis of the full 2024 deployment is currently ongoing; see [6] in these proceedings.

In order to apply the radar method to UHE neutrino detection, a detailed understanding of the properties of the radar signal is necessary; to help inform the layout of the future detector, and to aid the development of reconstruction techniques that best utilise the signal. Currently, two approaches towards modelling the signal have been developed. The first is RadioScatter [7], a MonteCarlo code package that calculates the radar return signal from a Geant4 particle cascade. Radioscatter has been used previously to investigate radar signal properties for different geometries [8, 9]. The second is MARES [10], a macroscopic semi-analytic code package that calculates the radar signal from parameterised, deterministic cascades. In this work, we use MARES to investigate radar signal properties in the RET-CR experiment, exploring how different features of the signal appear in this geometry.

2. Simulation Set-up

2.1 RET-CR Geometry

RET-CR employs both in-air and in-ice methods to detect incident CRs. The in-air components are detailed in [11]; here, we focus on the in-ice radar detection component of the experiment. As deployed, RET-CR used up to four amplified receivers situated in 10 m deep boreholes. Three of the receivers were positioned on a circle with a 30 m radius, centered around a phased-array transmitter encompassing $\sim$ 6 - 14 m depths [12]. Both the transmitter and receiver used wide-cylinder dipole antennas, operating in the 100 - 300 MHz frequency band [5].

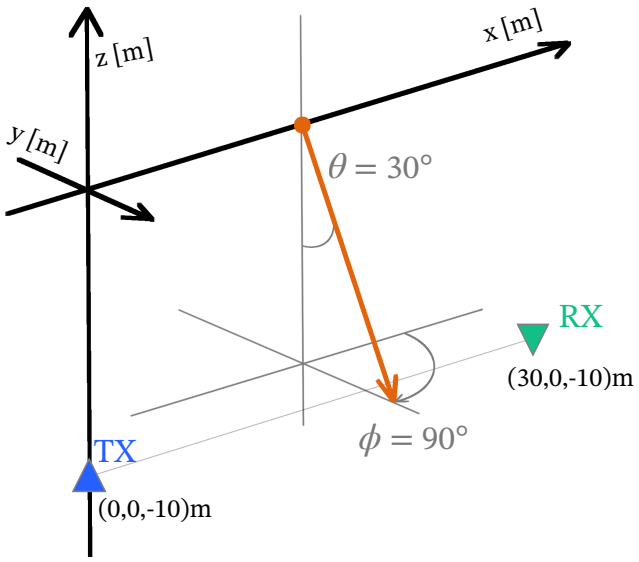

Figure 1: Detector layout setup within the MARES simulation, resembling the RET-CR experiment. An example cascade is signified with an orange arrow, with a zenith angle $\theta = 30°$ and an azimuth angle $\phi = 90°$.

2.2 MARES Simulation

A full description of MARES can be found in [10]. A brief overview is provided here: MARES employs NKG parameterisations to produce a particle cascade. The cascade is split into semi-circular segments, and the expected radar return power of each segment is found, through its radar cross section. The final receiver signal is then calculated as the sum of the signal contributions from all segments.

In this work, simulations are made for a single transmitter-receiver pair of vertically polarised antennas, separated by 30 m and both located 10 m deep, as shown in Figure 1. This reflects the positions of the transmitter and one receiver within RET-CR. Only a single receiver is used, as the radially symmetric nature of the in-ice detector, combined with the deterministic MARES code, ensures that signals for one antenna pair can be extrapolated to the full detector as needed. Currently, MARES uses a Hertzian dipole radiation pattern and a set peak gain in order to calculate the received voltage. The gain, transmit power and frequency were kept at constant values, with the transmit frequency set to 250 MHz to operate within the range of the RET-CR antennas.

The in-ice CR cascade is approximated as a neutrino-induced cascade originating from the x-y plane at $z = 0$ m, mimicking the ice surface. In [13], the in-ice energy deposit from CR air showers of different primary energies and zenith angles was investigated. For zenith angles below 50°, the energy deposits are found to be significantly reduced, making the detection of a secondary cascade difficult. Therefore, cascades are simulated with zenith angles θ between 0° to 50°, for all azimuth angles. This zenith range is chosen to encompass the majority of possible cascade directions that can occur, but does not take into account the expected distribution of CR zenith angles at the

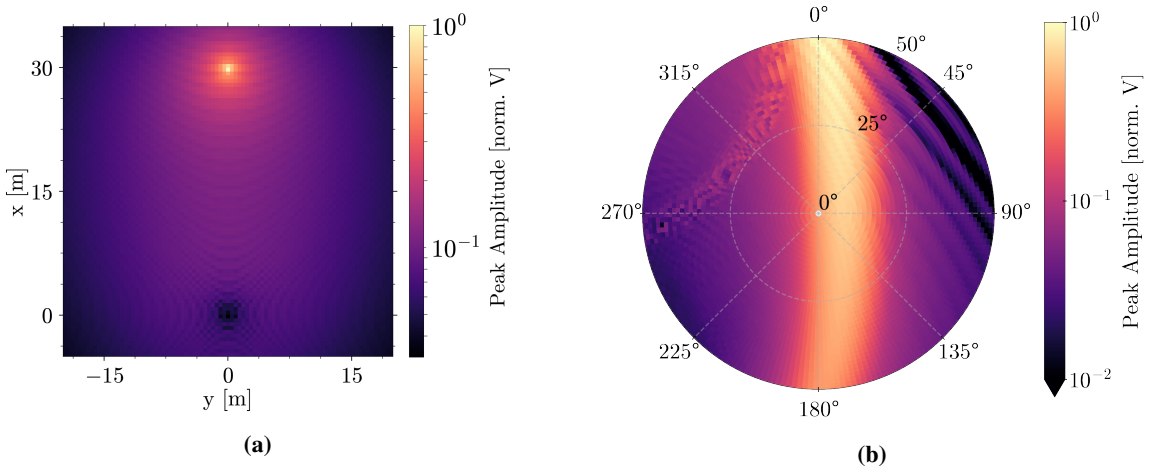

(a) **(b)**

Figure 2: **(a)** Simulated signal peak amplitudes for a grid of cascade positions. All cascades have a fixed arrival direction, moving vertically downwards with a zenith angle $\theta = 0°$. **(b)** Simulated peak amplitudes for a range of cascade arrival directions. Each cascade originates at a fixed position of (15,20) m on the surface. The zenith angle is plotted on the radial axis, and the azimuth as the polar angle; a cascade at the polar origin will have $\theta = 0°$, identical to each cascade in Figure 2a. Steeper showers are denoted by increased distance from the origin, up to zenith angles of 50°.

RET-CR site, which will in reality play a significant role in the range of signal properties seen. Similarly, the energy of the particle cascade is fixed at 20 PeV, chosen to approximately correspond to the in-ice energy deposit from a vertical CR air shower with a primary energy $E_p = 100$ PeV [13]. Finally, the ice volume is simulated with a constant refractive index $n = 1.78$, and density $\rho_{ice} = 0.917$ g/cm^3.

3. Signal Amplitude

In Figure 2a, the signal peak amplitude is shown for a grid of cascade positions originating from the ice surface. Cascades develop vertically downwards, away from the plane of origin. The transmitter and receiver positions are reflected in Figure 2a respectively as a bright and dark spot in the signal amplitude. Beyond these areas a fairly uniform distribution is seen, with a slow decrease at further distances from the two antennas, where the increased travel distance of the signal results in a lower peak amplitude.

Alternatively, in Figure 2b peak amplitudes for a range of cascade arrival directions are shown for a fixed position. The amplitude now exhibits a dependence on the arrival direction, where strongest signals are found for a distinct range of angles - seen in the bright vertical region. To explore this further, Figure 2b is remade for a selection of positions across the ice surface and plotted according to each position in Figure 3, producing a global view of the amplitude for both position and arrival direction. Allowing for some variation with distance, we see that the same bright region appears for nearly all positions, and we find that this feature can be correlated to the phase of the signals themselves.

For certain cascade directions, reflected signals from consecutive sections of the cascade arrive at the receiver mostly in phase with each other, causing their individual contributions to sum

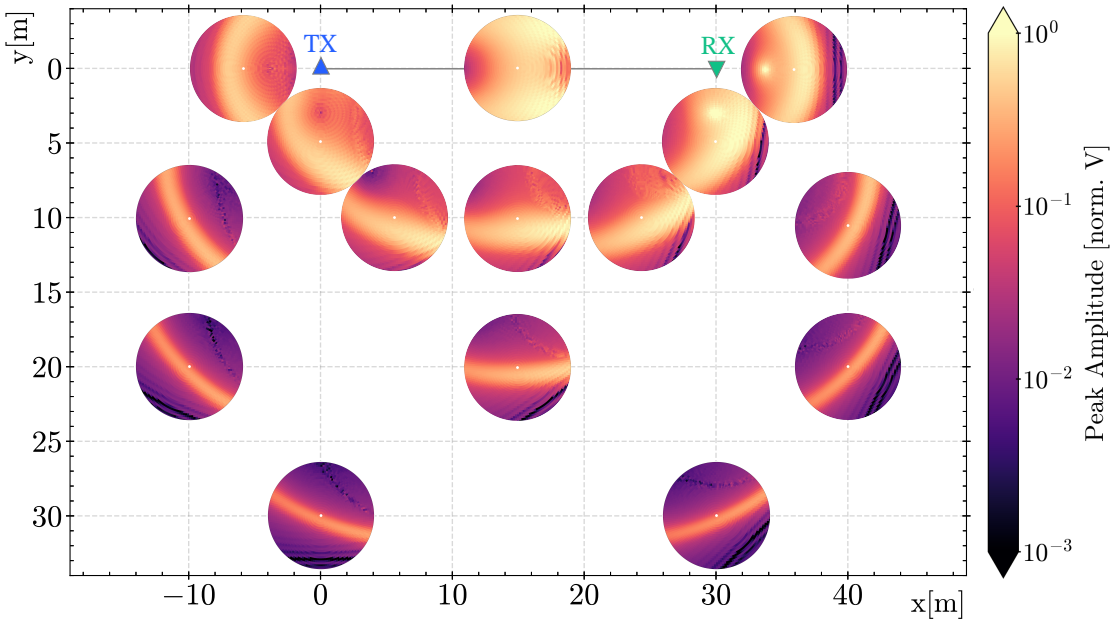

Figure 3: The received signal peak amplitude for a range of positions and arrival directions, sampled across the detector volume. Each individual plot is created at a fixed position, indicated by the location of the polar origin of each plot on the global map. For example, Figure 2b is located at (15,20) m. Arrival directions for each plot are indicated following Figure 2b.

coherently and produce a stronger signal. Varying the arrival direction will change the amount of phase coherence, influencing the received amplitude. In the bright regions in Figure 3, we see high amounts of phase coherence from the cascade. This effect was first presented in [14], and is explored further in [15] in these proceedings, where the signal amplitude is shown to be well-described by the amount of cascade phase coherence seen.

In the detector geometry of this work, we note that every vertical cascade shown in Figure 3 is found within the bright amplitude region. Therefore, the amplitude of vertical cascades within the simulated geometry - which includes all signals shown in Figure 2a - are primarily controlled by phase coherence. However, in Figure 3 this is no longer the case, and we see that the bright regions are curved with respect to the positions of both the transmitter and receiver. This demonstrates the geometry-dependence of phase coherence, influenced by both the transmitter-cascade and cascade-receiver angles, with the highest amplitudes found when the two angles are approximately equal.

4. Frequency Shifts

The signal frequency is investigated by taking the simulations presented in Figure 3 and instead plotting the peak frequency - the value corresponding to the strongest response in the frequency domain. This is shown in Figure 4, where it can be seen that the high amplitude regions described previously are echoed in the frequency domain, with the reflected signal frequency corresponding to the transmit frequency. At directions beyond these regions, the observed frequency changes compared to the transmit frequency, and Doppler shifting start to become apparent; cascades

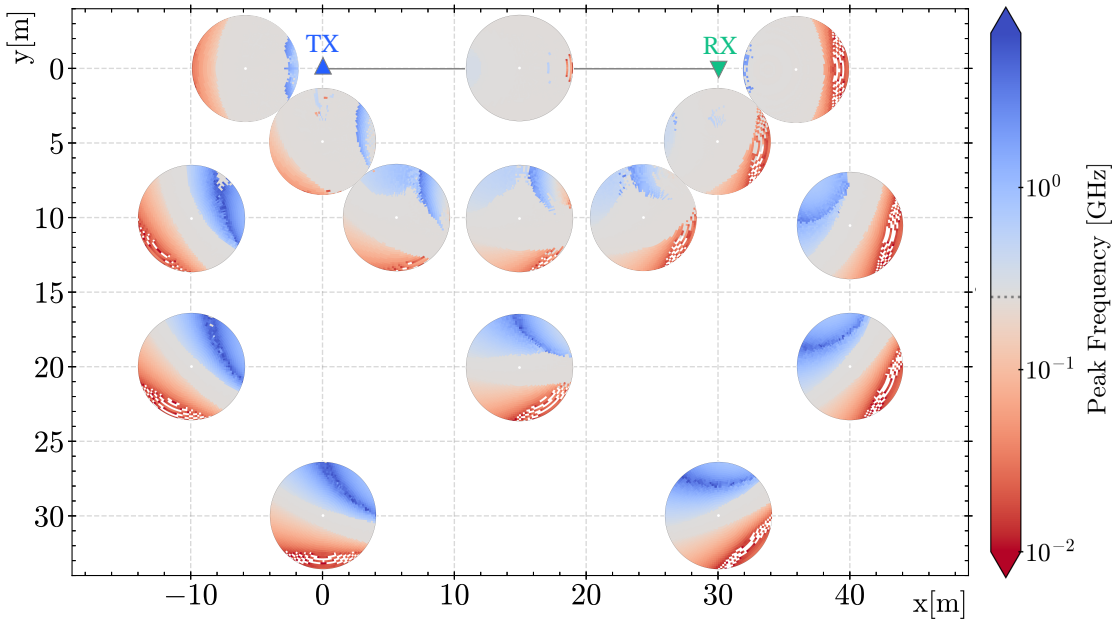

Figure 4: The peak frequency of signals for a range of positions and arrival directions situated around the detector. The transmit frequency is indicated with a dashed line on the colourbar, at the simulation value used (0.25 GHz).

moving towards the antennas produce upshifted signals, whereas cascades moving away lead to downshifts. The magnitude of these shifts intensify with direction until reaching either a distinct minimum downshift, or maximum upshift.

In the latter case, this is caused by a majority of the separate cascade signal contributions arriving simultaneously at the receiver, producing a very high frequency signal. This phenomenon can occur because the cascade develops at relativistic speeds, whereas the radar signal travels according to the medium velocity, producing a ring feature similar to the once caused by Cherenkov effects. Consequently, the direction that we find this effect is largely controlled by the refractive index of the medium. Considering the angle between the receiver and the cascade velocity, this ring is observed at the Cherenkov angle for ice in these simulations.

Although radio Askaryan emission is not included in this work, this feature in the radar signal also represents the region in which Askaryan emission could be expected from the in-ice cascade - which reaches a maximum at the Cherenkov angle of the medium [13]. Conversely, in the radar signal amplitude, strongest signals are not found at the Cherenkov ring. However, the presence of the transmitter antenna leads to the production of a second Cherenkov effect, responsible for the minimum peak frequencies seen in Figure 4. This feature occurs when the angle between the transmitter and the cascade velocity reaches the supplementary Cherenkov angle. In this case, destructive interference is seen, producing both low frequencies and amplitudes that appear as diffraction bands.

Work is currently ongoing to characterise the Doppler shifts, so that the expected shift can be predicted from the cascade arrival direction for a specific geometry. The extent of the frequency shifts seen in Figure 4 suggests that the radar signal frequency is very sensitive to the cascade arrival

direction, and could serve as a handle for future direction reconstruction.

5. Conclusion

Properties of the radar echo signal from in-ice cascades have been explored for a detector geometry resembling the RET-CR experiment. Signal amplitudes are found to be related both to the cascade position on the ice surface and to its arrival direction due to a phase coherence effect: A cascade developing at a favourable detector angle will benefit from signal contributions from different parts of the cascade adding coherently, boosting the amplitude and transmit frequency component of the total received signal. For directions where this is not the case, received signals are Doppler shifted, reaching very high frequencies at a receiver angle near the Cherenkov angle of the ice medium, and very low frequencies at the reflection of this angle from the transmitter. These properties provide insight into the expected radar signal in RET-CR, which can be built on in future work using more realistic ice profiles and cascades to better match the experiment as deployed.

References

[1] M. Ackermann, M. Bustamante, L. Lu, N. Otte, M.H. Reno, S. Wissel et al., *High-energy and ultra-high-energy neutrinos: A Snowmass white paper*, *Journal of High Energy Astrophysics* **36** (2022) .

[2] S. Prohira, K. de Vries, D. Besson, A. Connolly, C. Hast, U. Latif et al., *Suggestion of coherent radio reflections from an electron-beam induced particle cascade*, *Phys. Rev. D* **100** (2019) 072003.

[3] S. Prohira, K.D. de Vries, P. Allison, J. Beatty, D. Besson, A. Connolly et al., *Observation of Radar Echoes from High-Energy Particle Cascades*, *Phys. Rev. Lett.* **124** (2020) .

[4] Radar Echo Telescope collaboration, *The Radar Echo Telescope for Cosmic Rays: Pathfinder experiment for a next-generation neutrino observatory*, *Phys. Rev. D* **104** (2021) .

[5] Radar Echo Telescope collaboration, P. Allison, J. Beatty, D. Besson, A. Connolly, A. Cummings, C. Deaconu et al., *Initial performance of the Radar Echo Telescope for Cosmic Rays, RET-CR*, Sept., 2024. Submitted to Phys. Rev. D., arXiv:2409.07511 [hep-ex].

[6] D. Frikken et al., *The Radar Echo Telescope for Cosmic Rays: Contribution to ICRC 2025*, *PoS* **ICRC2025** (2025) no. 830.

[7] S. Prohira and D. Besson, *Particle-level model for radar based detection of high-energy neutrino cascades*, *Nucl. Instrum. Methods Phys. Res. A* **922** (2019) .

[8] V. Lukic and K.D. de Vries et al., *From signal properties toward reconstruction for the Radar Echo Telescope for neutrinos*, *PoS* **ARENA2022** (2023) .

[9] D. Frikken et al., *The Radar Echo Telescope for Neutrinos: Contribution to ICRC 2023*, *PoS* **ICRC2023** (2023) .

[10] Radar Echo Telescope collaboration, *Macroscopic approach to the radar echo scatter from high-energy particle cascades*, *Phys. Rev. D* **109** (2024) 083012.

[11] K. Nivedita and K. Mulrey et al., *High Energy Cosmic Ray Reconstructions with surface stations of RET-CR*, *PoS* **ICRC2025** (2025) no. 848.

[12] R. Stanley et al., *The Radar Echo Telescope for Cosmic Rays: Contribution to ICRC 2023*, *PoS* **ICRC2023** (2023) .

[13] S.D. Kockere, K.D. de Vries, N. van Eijndhoven and U.A. Latif, *Simulation of in-ice cosmic ray air shower induced particle cascades*, *Phys. Rev. D* **106** (2022) .

[14] K.D. de Vries, J. Loonen, I. Loudon, D. Frikken, E. Huesca Santiago, K. Mulrey et al., *Modeling and understanding radar echos from particle cascades*, *PoS* **ARENA2024** (2024) 011.

[15] J. Loonen et al., *Neutrino Event Properties and Reconstruction for the Radar Echo Telescope*, *PoS* **ICRC2025** (2025) no. 707.

Full Author List: RET Collaboration (June 16, 2025)

P. Allison[1], J.J. Beatty[1], D.Z. Besson[2], A. Connolly[1], A. Cummings[3,4,5], C. Deaconu[6], S. de Kockere[7], K.D. de Vries[7], I. Esteban[8], D. Frikken[1], C. Hast[9], E. Huesca Santiago[10], C.-Y. Kuo[11], A. Kyriacou[2], U.A. Latif[7], J. Loonen[7], I. Loudon[13], V. Lukic[7], C. McLennan[2], K. Mulrey[12], J. Nam[11], K. Nivedita[12], S. Prohira[2], J.P. Ralston[2], M.F.H. Seikh[2], R.S. Stanley[7], J. Stoffels[7], S. Toscano[13], D. Van den Broeck[7], N. van Eijndhoven [7], S. Wissel[4]

[1] Dept. of Physics, Center for Cosmology and AstroParticle Physics, The Ohio State University, Columbus, OH 43210
[2] Dept. of Physics and Astronomy, University of Kansas, Lawrence, KS 66045
[3] Center for Multi-Messenger Astrophysics, Institute for Gravitation and the Cosmos, Pennsylvania State University, University Park, PA 16802
[4] Dept. of Physics, Pennsylvania State University, University Park, PA 16802
[5] Dept. of Astronomy and Astrophysics, Pennsylvania State University, University Park, PA 16802
[6] Dept. of Physics, Enrico Fermi Institute, Kavli Institute for Cosmological Physics, University of Chicago, Chicago, IL 60637
[7] Vrije Universiteit Brussel, HEP@VUB, IIHE, Brussels, Belgium
[8] Department of Physics & EHU Quantum Center, University of the Basque Country UPV/EHU, PO Box 644, 48080 Bilbao, Spain
[9] SLAC National Accelerator Laboratory, Menlo Park, California 94025, USA
[10] Deutsches Elektronen-Synchrotron DESY, Platanenallee 6, 15738 Zeuthen, Germany
[11] Dept. of Physics, Grad. Inst. of Astrophys., Leung Center for Cosmology and Particle Astrophysics, National Taiwan University, Taipei, Taiwan
[12] Department of Astrophysics/IMAPP, Radboud University, P.O. Box 9010, 6500 GL Nijmegen, The Netherlands
[13] Université Libre de Bruxelles, Science Faculty CP230, B-1050 Brussels, Belgium

PoS(ICRC2025)1104

Acknowledgements

We recognize support from The National Science Foundation under Grants No. 2012980, No. 2012989, No. 2306424, and No. 2019597 and the Office of Polar Programs, the Flemish Foundation for Scientific Research FWO-G085820N, the European Research Council under the European Unions Horizon 2020 research and innovation program (Grant Agreement No. 805486), the Belgian Funds for Scientific Research (FRS-FNRS), IOP, and the John D. and Catherine T. MacArthur Foundation. Isha Loudon is a FRIA grantee of the Fonds de la Recherche Scientifique-FNRS.